2009

Influence of shielding gas on fume formation rate for gas metal arc welding (GMAW) of plain carbon steel

Kristin R. Carpenter
University of Wollongong, kristinc@uow.edu.au

Brian J. Monaghan
University of Wollongong, monaghan@uow.edu.au

John Norrish
University of Wollongong, johnn@uow.edu.au

Publication Details

Carpenter, KR, Monaghan, BJ & Norrish, J, Influence of shielding gas on fume formation rate for gas metal arc welding (GMAW) of plain carbon steel, Trends in Welding Research - Proceedings of the 8th International Conference, 2009, p 436-442, OH 44073-0002, United States: ASM International.

Trends in Welding Research, Proceedings of the 8th International Conference
Stan A. David, Tarasankar DebRoy, John N. DuPont, Toshihiko Koseki, Herschel B. Smartt, editors, p 436-442
DOI: 10.1361/cp2008twr436

www.asminternational.org

Influence of Shielding Gas on Fume Formation Rate for Gas Metal Arc Welding (GMAW) of Plain Carbon Steel

K.R. Carpenter, B.J. Monaghan and J. Norrish
University of Wollongong, Australia

Abstract

Shielding gas composition is an important parameter for successful gas metal arc welding (GMAW) and has been shown to affect the fume formation rate (FFR). The present paper compares thirteen shielding gases and their impact on FFR in spray transfer.

In Ar-based mixtures, increasing CO_2 had a greater impact than raising O_2 on FFR. When O_2 was increased in ternary mixtures, the FFR increased for Ar-5%CO_2 but no discernable increase was observed for the Ar-12%CO_2 mixtures. Ar-He-CO_2 mixtures had the most stable FFR's. The FFR for 100% CO_2 was significantly higher due to the change in weld transfer mode to globular and increased spatter. Results indicate that CO_2 additions in Ar-based shielding gases are the controlling factor in determining FFR due to the effect of CO_2 on welding arc characteristics. There was no obvious influence from the shielding gas on particle composition and fume particles were identified as $(Fe,Mn)_3O_4$.

Introduction

Gas metal arc welding (GMAW) is an important industrial process used for the joining of metals. The generation of welding fumes during arc welding processes is inevitable and are potentially hazardous to the welder's health. Welding fumes consist of metal oxide particles that can remain suspended in the air and thus, inhaled by welders.[1-3] The chemical composition and particle size of the fume particulates are important parameters in determining the toxicity of welding fumes.[3, 4]

The chemical composition and the fume formation rate (FFR) depends on several factors, namely, the welding parameters and processes, the filler and base materials and the shielding gas.[5-7] Due to the high temperatures involved with the welding arc, metal vapours are thought to predominately originate from the molten tip of the welding electrode[8], though the molten weld pool is also a significant source.[1, 6] Metal vapours are readily oxidised and rapidly condense into nano-sized particles.

The critical factors controlling the FFR are the arc current and voltage[1, 3, 5], arc temperature, surface area of the wire tip and the size of droplets exposed to the arc hot zone.[9, 10] The oxygen content of the shielding gas, the proportion of CO_2 and O_2, directly affects the FFR.[5, 11] In particular, FFR increases with increasing CO_2 additions in Ar-based shielding gases.[3, 5, 12] This observation is consistent with Turkdogen's oxidation enhanced evaporation model for steelmaking fumes[13, 14], where metal vapour reacts with oxygen near the surface of the metal, forming oxide and as a consequence enhancing fume formation. Ioffe et al[10], based on Turkdogen's oxidation enhanced evaporation model, suggested that oxidation of liquid iron on the droplet surface, as opposed to oxidation of iron vapour, would occur if the oxygen concentration exceeded a critical concentration of approximately 10%. However, Dennis et al[15] report that oxidation enhanced vaporisation would be unlikely to occur due to the large temperature variation between the molten droplet and the surrounding plasma, as well as the extremely high temperatures involved.

This paper will address the influence of the shielding gas on the chemical composition and FFR of welding fumes generated by robotic GMAW of plain carbon steel. TEM-EDS analysis was used to determine the chemical compositions of the fume particles and X-Ray diffraction (XRD) to identify the bulk phases of the fume.

Experimental Procedures

Gas metal arc welding (GMAW) of plain carbon steel (10 mm thick) was carried out with a Cigweld Trans Robot WS-0550 linked to a Fronius Trans Synergic 4000 power supply and wire feed system. The welding parameters were; AWS A5.18 (ER70S-6) uncoated, 1.2 mm diameter wire, 32 volts, wire feed rate 8 m min^{-1}, contact tip to work distance (CTWD) of 20 mm, gas flow rate of 20 L min^{-1}, weld travel speed of 300 mm min^{-1} and direct current (electrode positive). Using the above welding parameters typically produced currents of 280 ± 10 A. The welding parameters were chosen to achieve spray transfer for all shielding gases except 100% CO_2, which inherently operates in a globular mode. For 100% CO_2, three voltages were used, 32 V, 34 V and 36 V, to investigate the effect of increasing arc voltage on FFR. The nominal chemical composition of the base plate and welding wire are shown in Table 1.

Table 1: Nominal chemical composition (wt%) of the base plate and welding wire.

	C	Mn	Si	Fe	Mn/Fe
Base plate	0.22	1.6	0.55	97.63	0.016
AWS A5.18	0.08	1.16	0.7	98.06	0.012

A WITT KM 30-4 gas mixer was used to generate the shielding gas mixtures listed in Table 2. In Table 2, results are also given for; FFR, oxygen index and the TEM-EDAX results. The oxygen index was calculated using the simple IIW (International Institute of Welding) empirical formula, ($\%O_2$ + 0.5$\%CO_2$), which was used to estimate the 'oxidising effect' of the shielding gas.[16, 17] This 'oxidising effect' is generally referred to as 'oxygen potential' in welding literature. The above formula was based on oxygen analysis of weld metal. Gas-weld metal interactions are much better characterised and understood than fume condensation and fume condensate-gas systems in welding. Given our uncertainty of the reactions taking place, the species present and the prevailing reaction temperature the usefulness of such a function is limited. Oxygen index is used here simply as a basis for comparison.

A Platon flowmeter was placed between the gas mixer and welding machine to ensure a constant flow-rate. The flow meter was calibrated with air using a water displacement test, where the flow rate was calculated by measuring the time taken for a given volume of water to be displaced by the gas. The flow meter reading was then corrected for the selected gas composition using gas density corrections, by using Equation 1.

$$F_{gas} = \frac{F_{air}}{k}, \qquad k = \sqrt{r} \qquad (1)$$

Where F_{gas} is the flow rate of the selected gas, F_{air} is the flow rate for air and k is a constant based on the relative gas density to air, r, at constant temperature and pressure. The values used for, r, were; Ar 1.380, CO_2 1.520, He 0.138 and O_2 1.105 and ideal gas-mixing was assumed to calculate the density for each gas mixture.

Table 2: Shielding gas mixtures used for robotic GMAW, FFR results, O_2 index and average particle composition.

Gas composition	FFR (g min^{-1})	O_2 Index	O (wt%)	Si (wt%)	Mn (wt%)	Fe (wt%)	Mn/Fe
Ar-5%O_2	0.274	5%	27.5	0.9	8.7	62.8	0.14
Ar-5%CO_2	0.246	2.5%	27.5	0.7	7.0	64.8	0.11
Ar-10%CO_2	0.298	5%	27.4	0.3	5.9	66.4	0.09
Ar-18%CO_2	0.396	9%	28.1	1.3	4.2	66.3	0.06
Ar-5%CO_2-2%O_2	0.242	4.5%	27.5	0.6	7.4	64.5	0.12
Ar-12%CO_2-2%O_2	0.312	8%	27.8	1.0	5.8	65.3	0.09
Ar-18%CO_2-2%O_2	0.392	11%	28.4	2.3	7.0	62.3	0.12
Ar-5%CO_2-5%O_2	0.352	7.5%	28.1	1.6	6.1	64.2	0.10
Ar-12%CO_2-4%O_2	0.318	10%	28.1	1.6	6.1	64.2	0.10
Ar-12%CO_2-6%O_2	0.332	12%	-	-	-	-	-
Ar-20%He-12%CO_2	0.279	-	28.1	1.3	4.0	66.6	0.06
Ar-30%He-6%CO_2	0.273	-	27.7	0.8	6.1	65.4	0.10
Ar-30%He-10%CO_2	0.277	-	27.7	0.8	4.8	66.8	0.07
100% CO_2 (32V)	0.568	-	29.6	4.4	6.5	59.4	0.11

A 255 mm long bead was welded onto a plain carbon steel plate in a fume box and fume was collected for TEM analysis on an aluminium SEM stub. The stub was in a fixed position 30 mm from the centre line of the arc in the welding direction and 50 mm above the plate. This position was chosen to provide sufficient fume collection for TEM analysis, as determined from previous work.[18] Chemical analysis was performed with TEM-EDS, using a Jeol JEM 2011 at 200 KV equipped with a Si(Li) detector, using a double tilt beryllium holder. Fume particles were washed off the stub by ultrasonic agitation into a bath of ethanol, where the ethanol was pre-filtered through 0.22 µm micro-pore filter to remove contaminates. This mixture was then deposited onto holey carbon-coated TEM copper grids.

For FFR determination, a shorter weld bead with an arc time of 20 seconds was used to prevent clogging of the filter paper. The fume box design originated from the recommendations of international standard ISO15011-1[19], but a number of modifications have been made to cater for the robot arm movement; sliding doors were fitted to the rear opening of the fume enclosure. Pall type A/E glass fibre filters were used, with a nominal pore size of 1 µm and a typical thickness of 330 µm. A Sartorius balance (Model CP225D) was used to

weight the filter paper before and after the test to obtain the mass of fume generated to five decimal places. FFR was expressed as the weight of fume generated per unit of arc time (g min^{-1}) and is the mean of three measurements for each test. Over the entire test range, the majority of measurements had a scatter of less than ± 3.7%.
The maximum scatter was ± 7.6% around the mean and is consistent with FFR measurements made to international standard ISO15011-1.

A GBC Scientific Equipment, MMA X-ray diffractometer was used to identify bulk phases in the fume. Fume was transferred onto a low-background quartz slide, where a thin layer of petroleum jelly was used to adhere the fume to the slide. Scans were conducted from 15° to 75° 2θ at a rate of 1° min^{-1}, step size 0.02 and with the X-ray source running at 1.0 kW (35 kV and 28.8 mA).

Results

XRD

XRD analysis of the (bulk) fume identified the Fe_3O_4 -spinel type phase (Magnetite-index card 011-0614 ICDD data base). There was no evidence that shielding gas composition affected the composition of the bulk fume. There was a slight peak shift that indicated that small levels of Mn, as detected by TEM-EDS, substituted for Fe in the Fe_3O_4 phase. This is consistent with other studies reported in the literature.[20, 21]

TEM – EDS

The average composition determined by TEM-EDS for a number of particles for each shielding gas mixtures are included in Table 2. Fume particles were composed mainly of Fe-oxide (Fe_3O_4) and contained a small amount of Mn and trace amounts of Si.

EDS results showed that small peaks of Si and O were present in the background when the electron beam was focused on the carbon film. It is likely that the trace amounts of Si and O, about 0.2-0.5 wt%, were at least in part from O-ring grease contamination from TEM sample holders. The presence of Si in fume particles is widely known but with this background contamination it is impossible to accurately determine the amount of Si in the fume particles. Results suggest that Si levels in the fume were similar to the wire composition. However, significant Mn enrichment of the fume was observed.

Fume Morphology

Typical TEM images are shown in Figures 1 and 2. Figure 1 shows a mixture of spherical and faceted particles, including the tendency of the particles to agglomerate in groups and chain-like structures. Figure 2 shows the less frequent rhombohedral particle morphology. In Figure 2, lattice fringes are clearly visible indicating the crystalline structure of the fume particle. The inset image shows the d-spacing, measured at 0.48 nm, which matched that (0.485 nm) of the Fe_3O_4 - spinel Magnetite phase identified using XRD. The zero order [1,1,1] direction has hexagonal 6mm symmetry, as can be seen in the inset of Figure 2, but it should be noted that a cubic structure only will have 3mm symmetry. TEM observations yielded no evidence of metal core - oxide shelled particles that have previously been reported in the literature.[22]

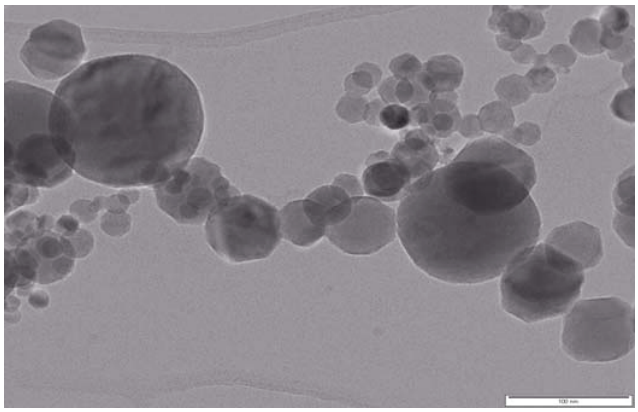

Figure 1: Typical bright field TEM image showing welding fumes with a mixture of particle sizes, with either spherical or faceted morphology and often in chain-like structures.

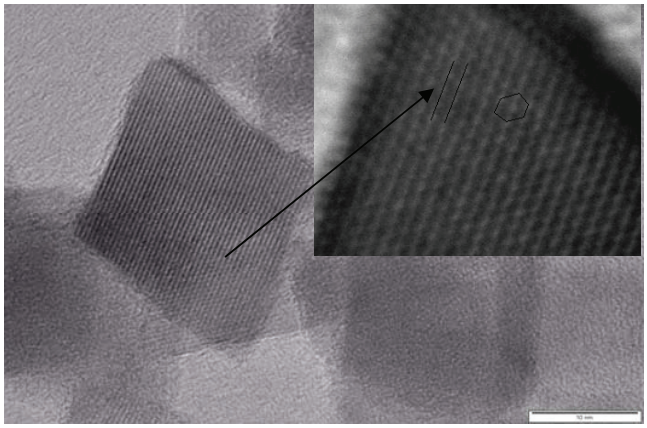

Figure 2: Typical bright field TEM image showing welding fume particles with rhombohedral morphology and lattice fringes. The inset image is at higher magnification, showing the lattice fringes more clearly.

Fume Emissions

Fume formation rate is plotted as a function of shielding gas composition in Figure 3. Each region on the graph groups FFR results according to different variables of the composition of the shielding gas mixtures. For Ar-5%O_2, FFR increased slightly over that for Ar-5%CO_2 but was less than that for Ar-10%CO_2, the binary CO_2 mixture with the equivalent oxygen

index. FFR increased with increasing CO_2 for the binary Ar-CO_2 mixtures.
In the ternary CO_2 + 2%O_2 mixtures, FFR also increased with increasing CO_2 but the addition of 2%O_2 had no impact on the FFR when compared to equivalent binary mixtures. When the O_2 was increased in the ternary mixtures, the FFR increased at the 5%CO_2 level but at 12%CO_2, given the scatter in experimental data, there was no discernable increase. For the He group, there was no significant change in the FFR indicating that minor CO_2 and/or He variations have an insignificant influence.

Fume formation rate as a function of oxygen index for the Ar-O_2, Ar-CO_2 and Ar-CO_2-O_2 series is plotted in Figure 4. From Figure 4, a weak trend of FFR increasing with oxygen index was observed.

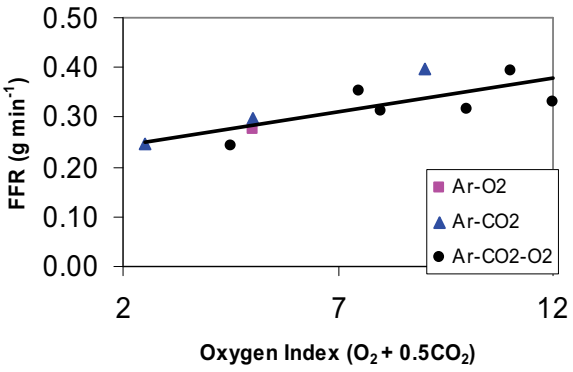

Figure 4: FFR plotted against oxygen index for the Ar-O_2, Ar-CO_2 and Ar-CO_2-O_2 series.

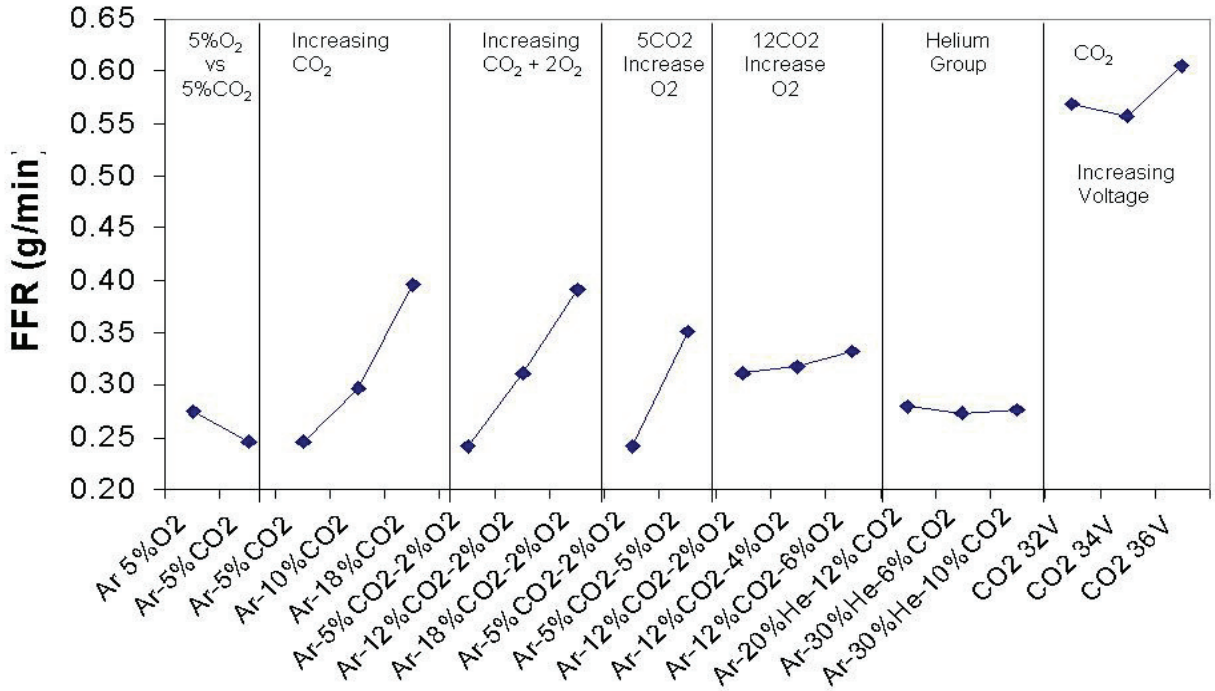

Figure 3: FFR as a function of shielding gas composition under the same welding conditions. Each region on the graph groups the shielding gas mixtures according to different variables in the composition.

Discussion

The results presented in Figures 3 and 4 show several anomalies to the view that FFR is a function of the oxygen index of the shielding gas. Firstly, there was no discernable increase in FFR for the Ar-12%CO_2 ternary mixtures when oxygen was increased from 2% to 6%. This corresponds to a large increase in the oxygen index of 50%. If oxygen index was the controlling factor, it would be reasonable to expect that a 50% increase would yield a noticeable increase in FFR. Secondly, the addition of 2% oxygen to the Ar-CO_2 mixtures had no influence on FFR. This is illustrated more clearly in Figure 5, where the FFR results for Ar-CO_2 and Ar-CO_2-2%O_2 showed identical curves. Figure 4 showed a weak trend of increasing FFR with increasing oxygen index and considerable scatter.

The argument for oxygen index controlling FFR was essentially based on Turkdogan's et al[13] oxidation enhanced vaporisation work. The rate of evaporation from molten metal was estimated from the Langmuir equation when derived in a vacuum, which gives the maximum possible evaporation rate.

$$J\max = \frac{p}{\sqrt{2\pi RTM}} \qquad (2)$$

Where p is pure vapour pressure, R is the gas constant, T is temperature (K) and M is the molar weight of the metal vapour.

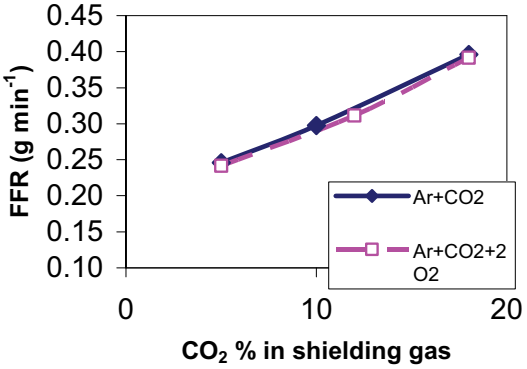

Figure 5: FFR plotted as a function of CO_2 in shielding gas for Ar-CO_2 and Ar-CO_2-2%O_2.

For a given temperature, the rate of vaporisation (fume formation) will increase with increasing partial pressure of oxygen in the atmosphere (oxygen index). Therefore, increasing the amount of active components in the shielding gas could enhance fume formation but results have shown that this does not always take place.

The Langmuir equation is also dependent on temperature and it is feasible that temperature is the controlling factor in determining the FFR. An increase in the surface temperature of a droplet has been shown to be a critical controlling factor in fume formation.[1, 9, 10, 23] Droplet size is also a key factor in determining FFR for two main reasons; 1) increased surface area available for vaporisation and 2) increasing droplet size tends to increase droplet temperature.[9, 23]

Figure 5 shows that FFR was a function of the %CO_2 in argon based shielding gases. Pires[24] also found that CO_2 additions had a stronger influence on FFR than oxygen additions. It is proposed that it is the effect of CO_2 on weld metal transfer and arc characteristics, not just the increase in oxygen index, that is responsible for higher FFR's. It is known that increasing CO_2 levels in argon based shielding gases tends to reduce arc stability.[25] For example, Pires et al[24] produced transfer maps for different shielding gas mixtures and found that arc stability decreased with increasing CO_2 for binary mixtures. Rhee and Kanateyasibu[26] discovered that droplet size increased as the %CO_2 in argon increased over a range of currents (242-342A). An increase in droplet size and consequently, an increase in droplet surface temperature, would enhance fume formation. Further work, such as high speed videography of the welding arc, would be required to confirm this mechanism.

The FFR of 100% CO_2 was approximately double the Ar-based mixtures which is consistent with the well know higher FFR's for globular transfer. The relatively large, turbulent droplets and long detachment times for globular transfer compared to spray transfer, as well as fume from spatter, will enhance vaporisation.[1, 5] In Figure 3 it can be seen that FFR increased for 100% CO_2 with increasing arc voltage. Increasing the arc voltage increases the arc temperature and the length of the arc, both of which promote increased vaporisation and hence, fume formation.

Fume Composition

The combination of TEM-EDS with XRD revealed that Fe_3O_4 was the dominate phase. There was no evidence of MnO in XRD results, it is therefore expected that Mn substituted for Fe in the Fe_3O_4 structure. The Mn atom is of a similar size to that of Fe and is known to be able to substitute for Fe in solid solutions. The Fe_3O_4-Mn_3O_4 system is reproduced from the Slag Atlas[27] in Figure 6, showing extensive solubility of Mn in Fe_3O_4 (Cubic-$(Fe,Mn)_3O_4$ ss). The measured levels of Si in the fume are mostly below the detection capabilities of XRD so it is difficult to determine if Si was present in the form of a siliceous compound, such as SiO_2 or if Si was incorporated into the $(Fe,Mn)_3O_4$ structure. The Si atom is also similar in size to the Fe atom but has a higher valence of 4+, therefore according to the Hume-Rothery rules for solubility only partial solubility would be expected.[28] The uniform, crystalline nature of the fume particles (Fig. 2) and the detection of Mn and Si in all particles indicates that fume particles are $(Fe,Mn)_3O_4$ with trace Si additions.

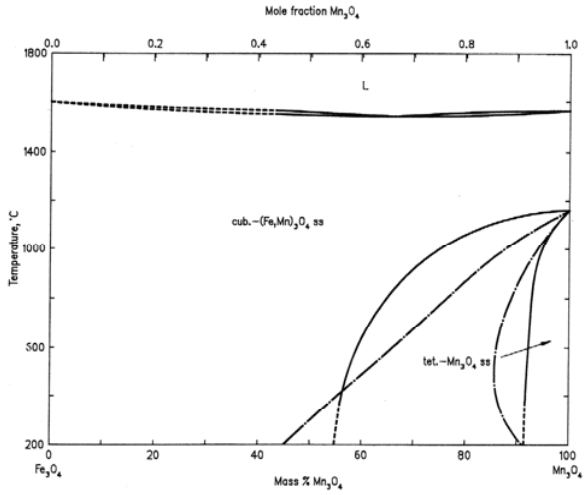

Figure 6: Fe_3O_4-Mn_3O_4 system, showing an extensive region of cubic $(Fe,Mn)_3O_4$ solid solution, reproduced from the Slag Atlas.[27]

The TEM-EDS results showed a wide range of scatter for the analysis of particles for different shielding gas compositions; no discernable trend was observed. This suggested that shielding gas has no apparent effect on particle composition, but the scatter may well be a reflection of variations in the composition of particles generated during welding. The exception was a noticeable increase in the Si level when welding with 100% CO_2 shielding gas. A more comprehensive analysis of fume particles would be required to determine if the shielding gas composition has any influence on fume composition and to determine if composition varies with particle size.

Conclusions

This paper studied the influence of shielding gas composition on FFR and particle composition for robotic GMAW of mild steel. Fume tests showed that FFR was strongly affected by increasing CO_2 additions for both binary and ternary Ar-CO_2-O_2 mixtures. The addition of 2%O_2 to binary Ar-CO_2 mixtures had no effect on FFR. When the O_2 was increased in the ternary mixtures, the FFR increased at the 5%CO_2 level but no discernable increase was observed for the 12%CO_2 mixtures. Increasing He or CO_2 in ternary Ar-He-CO_2 mixtures had little impact on the FFR. For 100% CO_2, FFR significantly increased due to globular transfer mode and high spatter levels.

The results obtained have shown that oxygen index only weakly correlates with FFR and therefore increasing the CO_2 addition in argon based shielding gases is the main factor controlling fume generation. This is attributed to the influence of CO_2 on metal transfer and arc characteristics.
The combination of TEM-EDS with XRD identified fume particles as $(Fe,Mn)_3O_4$ with additions of Si. It was found that shielding gas composition had no obvious effect on fume composition. Enrichment of Mn in the fume composition was observed.

Acknowledgement

The funding for this project was provided by Linde-BOC Gases, Australia.

References

1. H. R. Castner: *Welding Journal*, 74, 59--68-. (1995)
2. P. J. Hewitt: *Indoor Built Environment*, 1996, 5, 253-262.
3. V. Voitkevich: 'Welding fumes: Formation, properties and biological effects'; Cambridge, England, Abington Publishing. (1995)
4. P. J. Hewitt and A. A. Hirst: *Annals of Occupational Hygiene*, 1991, 35, 223.
5. R. F. Heile and D. C. Hill: *Welding Journal*, 54, 201-210. (1975)
6. Y. Jin: *Staub - Reinhaltung der Luft*, 54, 67. (1994)
7. Z. Sterjovski, J. Brossier, E. de Thoisy, D. Cuiuri, J. Norrish, and B. Monaghan: *Australiasian welding journal*, 51, 34-40. (2006)
8. M. Kobayashi, S. Maki, Y. Hashimoto, and T. Suga: *Welding Journal*, 62, 190-196. (1983)
9. R. T. Deam, S. W. Simpson, and J. Haidar: *Journal of Physics D: Applied Physics*, 33, 1393. (2000)
10. I. Ioffe, D. MacLean, N. Perelman, I. Stares, and M. Thornton: *Journal of Physics D: Applied Physics*, 28, 2473. (1995)
11. C. N. Gray, P. J. Hewitt, and R. Hicks: *Proceedings - Biennial Cornell Electrical Engineering Conference*, 1, 167. (1980)
12. D. E. Hilton and P. N. Plumridge: *Welding and Metal Fabrication*, 59, 555. (1991)
13. E. T. Turkdogan, P. Grieveson, and L. S. Darken: *J. Phys. Chem.*, 67, 1647-1654. (1963)
14. E. T. Turkdogan and L. E. Leake: *Journal of the Iron and Steel Institute*, June, 162-170. (1959)
15. J. N. Dennis, P. J. Hewitt, C. J. Redding, and A. D. Workman: *Ann. Occup. Hyg.*, 45, 105-113. (2001)
16. A. A. Smith: *Welding in the World*, 16, 25-30. (1978)
17. N. Stenbacka and K.-A. Persson: *Welding Journal*, 68, 41-47. (1989)
18. S. Zhou, J. Norrish, and Z. Chen: 'Influence of different metal transfer modes on welding fume generation during gas metal arc welding', Proceedings of Materials 98, The biennial conference of the Inst. of materials eng., 295-300.(1998)
19. ISO. standard: 'ISO 15011-1:2002: Health and safety in welding and allied processes - Laboratory method for sampling fume and gases generated by arc welding - Part 1: Determination of emission rate and sampling for analysis of particulate fume'; (2002)
20. N. T. Jenkins and T. W. Eagar: *Welding Journal*, 84, 87-s-93-s. (2005)
21. J. W. Sowards: *Welding in the World*, 50, 40.

22. P. Konarski, I. Iwanejko, and M. Cwil: *Vacuum*, 2003, 70, 385-389. (2006)
23. N. T. Jenkins, P. F. Mendez, and T. W. Eagar: 'Effect of arc welding electrode temperature on vapor and fume composition′, Proceedings of the International Conference: Trends in Welding Research, Pine Mountain, GA, United States, 491.
24. I. Pires, L. Quintino, and R. M. Miranda: *Materials and Design*, 28, 1623. (2007)
25. R. L. O'Brien and L. P. Connor: 'Welding Handbook', 133-136; Miami, AWS. (1991)
26. S. Rhee and E. Kannatey-Asibu: *Welding Journal*, 71, 381s-386s. (1992)
27. M. Allibert, H. Gaye, J. Gieseler, D. Janke, B. J. Keene, D. Kirner, M. Kowalski, J. Lehmann, K. Mills, D. Neuschutz, R. Parra, C. Saint-Jours, P. Spencer, M. Susa, M. Tmar, and E. Woermann: 'Slag Atlas', p73; Germany, Verlag Stahleisen GmbH. (1995)
28. J. Shackelford: 'Introduction to Materials Science for Engineers'; New York, Macmillian Publishing Company. (1992)